Journal of Medical Ultrasonics (2022) 49:545–553
https://doi.org/10.1007/s10396-022-01244-0

ORIGINAL ARTICLE–PHYSICS & ENGINEERING

The effect of attenuation inside the acoustic traps on the configuration of vertical artifacts in lung ultrasound: an experimental study with simple models

Toru Kameda[1] · **Naohisa Kamiyama**[2] · **Nobuyuki Taniguchi**[1]

Received: 7 May 2022 / Accepted: 22 June 2022 / Published online: 5 August 2022

Abstract

Purpose Using simple experimental models for lung ultrasound, we evaluated the relationship of the attenuation inside the sources of vertical artifacts to the echo intensity and attenuation of artifacts.

Methods As sources of artifacts, we made 10 different hemispherical gel objects with two different mediums (pure agar or agar containing graphite with an attenuation coefficient of 0.5 dB/cm · MHz) and five different diameters (3.6, 5.6, 7.5, 9.5, or 11.4 mm). Ten of each hemispherical gel object were prepared for the statistical analyses. Each object was placed onto a chest wall phantom as the plane of the hemisphere was placed in an upward position. The echo intensity and attenuation of the artifact generated from each object was measured and compared.

Results For all sizes, the intensity and attenuation of the artifacts in the objects made of agar containing graphite were significantly lower and larger, respectively, than those in the objects made of pure agar. In the objects containing graphite, the intensity decreased when the frequency was changed from 5 to 9 MHz.

Conclusion Based on this experiment, assessing the intensity and attenuation of vertical artifacts may help estimate the physical composition of sources of vertical artifacts in lung ultrasound.

Keywords Lung ultrasound · B-line · Vertical artifact · Experimental model · Attenuation

Introduction

In the international consensus statement published in 2012, B-lines in lung ultrasound are defined as discrete, laser-like vertical hyperechoic artifacts that arise from the pleural line and extend to the bottom of the screen without fading [1]. Considering their number and distribution in the lungs, B-lines are utilized for diagnosis, assessment of severity, and monitoring of cardiogenic pulmonary edema [2], acute respiratory distress syndrome [3], interstitial lung diseases [4, 5], bacterial pneumonia [6], and viral pneumonia including COVID-19 [7]. Even though the sonographic-pathologic correlations in B-lines have not yet been elucidated microscopically [8, 9], a large number of observational studies have indicated that B-lines are generated when the air content decreases and the lung density increases due to the presence of transudate, exudate, collagen, or hypercellularity in the subpleural space [10].

This prevalent definition of B-lines has some issues. Even though some vertical artifacts extend to the bottom of the screen when set at a shallow depth, they may not extend to the bottom of the screen when set at deeper depths. A recently published World Federation of Ultrasound in Medicine and Biology (WFUMB) position paper on reverberation artifacts in lung ultrasound recommends that the entire depth of the screen be at least 10 cm [11]. In addition, in contrast to B-lines, short vertical artifacts or vertical artifacts that do not reach the bottom of the screen have not received much attention in most clinical studies; however, these vertical artifacts are often observed in daily practice. They may also have clinical significance and provide information about the morphology and structure of the subpleural region [11, 12]. Furthermore, few

✉ Toru Kameda
kamekame@pb3.so-net.ne.jp

[1] Department of Ultrasound Medicine, Saiseikai Utsunomiya Hospital, 911-1 Takebayashi, Utsunomiya, Tochigi 321-0974, Japan

[2] Ultrasound Division, GE Healthcare Japan, 4-7-127 Asahigaoka, Hino, Tokyo 191-8503, Japan

clinical studies have analyzed the characteristics of vertical artifacts, such as the length, echo intensity, and attenuation, for differentiation of diseases in cases showing these artifacts [8, 13].

A hypothesis or theory concerning vertical artifacts followed by experimental studies would be useful for obtaining new insights concerning the sonographic-pathologic correlation and solving these issues regarding vertical artifacts. Lichtenstein et al. [14] first formulated a hypothesis regarding the formation of vertical artifacts in lung ultrasound in their early study. They mentioned that the ultrasound beam seemed to be "trapped" in a closed system, such as the sub-pleural end of the thickened interlobar septum, resulting in endless to-and-fro echoing. Soldati et al. [15] then introduced the theory of "acoustic trap" in the generation of vertical artifacts based on a series of clinical and experimental studies. An acoustic trap corresponds to the thickened interlobar septa, a small volume of fluid, and an inflammatory change surrounded by aerated alveoli in the subpleural space. Once an ultrasound beam enters the acoustic trap through the channel at the pleurae, it is trapped and reflected by the wall of aerated alveoli repeatedly with scattering. These phenomena act as successive ultrasound sources, with the trapped energy continuously radiating to the transducer.

To confirm this theory and obtain new insights, we developed simple experimental models that easily generate vertical artifacts [9, 16]. The results obtained from the models supported the trap theory and indicated that the length and echo intensity of the vertical artifacts depended on the relative size of the channel and the relative height of the trap to the trap volume [16]. The theory was also supported by another experimental study using agar cusps and simulated interlobular septa as models of acoustic traps [17].

In our previous study [16], we used materials with acoustic properties similar to water as sources of vertical artifacts. This model seemed suitable for considering the mechanism underlying the B-lines in cardiogenic pulmonary edema, where a rapid increase in hydrostatic pressure in capillaries leads to increased fluid transfer into the interstitium and alveolar spaces. If a material with significant sound attenuation is substituted for materials with similar properties to water as the source of vertical artifacts, the intensity and attenuation of the vertical artifacts may be lower and larger, respectively. This model may be suitable when considering the mechanism underlying vertical artifacts in pulmonary diseases, such as interstitial lung diseases [16], based on the assumption that the vertical artifacts may be generated by acoustic traps mainly consisting of collagen and cells in these diseases [13].

Given the above, we conducted another experimental study using a diagnostic ultrasound scanner to confirm this hypothesis based on a preliminary report [18].

Methods

This experimental study was performed based on common settings of diagnostic scanners and using the simple models introduced in our previous article [16]. The experiment was performed using a commercially available ultrasound scanner (LOGIQ S8; GE Healthcare, Tokyo, Japan) with a 9-MHz linear transducer (9L-D).

Table 1 show the settings of the ultrasound scanner, which were the same as the ones in our previous study, except for the frequency [16]. The depth of the screen was set at 10 cm based on clinical usage recommended in the WFUMB position paper [11]. A single focal point was set at the distance from the footprint of the transducer to the object being used as the source of a vertical artifact to emphasize the artifact and keep the artifact as narrow as possible [9, 18, 19]. Spatial compound imaging was turned off to avoid generating multiple linear artifacts from the object [9, 18]. The dynamic range was set at 72 dB, which is slightly wider than the range used in clinical settings. The sliders for the time gain compensation (TGC) on the scanner were kept in the central position. Post-processed image filters, such as frame average and speckle reduction, were set to zero or the minimum.

The probe was fixed with the footprint facing upward. A polypropylene sheet 0.008 mm in thickness and a small block of bacon 2.5 cm in height as a chest wall phantom were placed on the footprint in that order. We selected this chest wall phantom because the image was similar to real chest wall images. A thin layer of ultrasound gel (LOGIQLEAN gel hard; GE Healthcare, Tokyo, Japan) was used as the coupling medium between the footprint and the polypropylene sheet and between the sheet and the phantom. The probe and phantom were then immobilized using adhesive tape.

We made 10 different hemispherical gel objects with two different mediums and five different diameters using molds (Fig. 1). A hot solution made of de-aerated water and powdery agar (3%) was poured into commercially available

Table 1 Settings of ultrasound scanner LOGIQ S8 with a 9L-D linear transducer

Setting	Value
Frequency	5, 9 MHz
Depth of screen	10 cm
Focal point (single focus)	2.5 cm
Spatial compound imaging	Off
Tissue harmonic imaging	Off
Gain	60
Dynamic range	72
Frame average	0

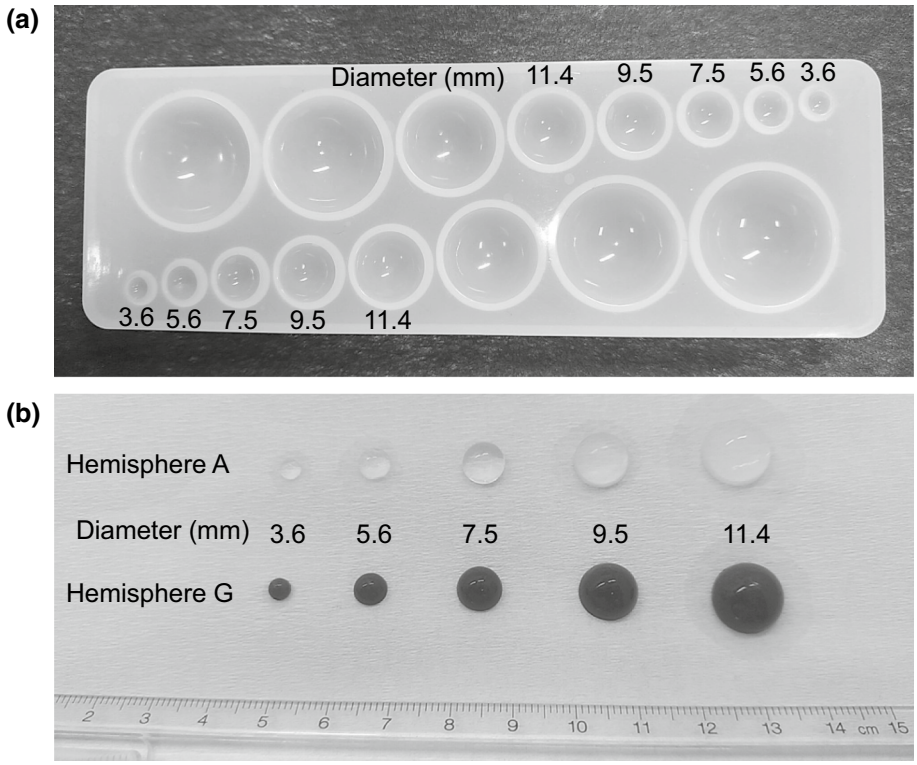

Fig. 1 A photograph of a commercially available silicone mold (**a**) and a photograph of 10 different hemispherical gel objects laid on a sheet as the planes (cross sections) make contact with it (**b**). Hemisphere A is a hemispherical gel object made of water and agar. Hemisphere G is a hemispherical gel object made of water, agar, and graphite

silicone molds (Shop Sasuke, Aichi, Japan) with a disposable dropper to make hemispherical objects 3.6, 5.6, 7.5, 9.5, and 11.4 mm in diameter. A hard polypropylene sheet was then placed on top of each mold to eliminate the swelling of the solution due to surface tension. Once the agar models had cooled and set, they were removed from the molds. We obtained 10 hemispherical objects at each diameter for the experiment. The hemispherical objects made of water and agar were named "hemisphere A".

Next, hemispherical gel objects containing powdery graphite (Wako Pure Chemical Industries, Osaka, Japan) were made. A hot solution made of de-aerated water, powdery agar (3%), and graphite (5%) was poured into the molds to make hemispherical objects 3.6, 5.6, 7.5, 9.5, and 11.4 mm in diameter in the same way as described above. We obtained 10 hemispherical objects at each diameter for the experiment. The hemispherical objects made of water, agar, and graphite were named "hemisphere G". The attenuation coefficient of hemisphere G was 0.5 dB/cm · MHz, which is similar to that of soft tissue in general. We prepared 10 samples of hemisphere A and G at each diameter for a total of 100 hemispherical objects.

A polypropylene sheet 0.008 mm in thickness was laid onto the chest wall phantom, which was coated with a thin layer of ultrasound gel. A hemisphere A 3.6 mm in diameter was then placed onto the sheet through a thin layer of ultrasound gel as the plane (the cross section) of the hemisphere was placed in an upward position, sharing the point of contact between the spherical surface and the sheet through the thin layer of ultrasound gel. We observed the vertical artifact generated by hemisphere A and recorded the still images at 5 MHz and then 9 MHz. In the same manner, we observed and recorded the vertical artifacts generated from the other hemispherical objects in the following order: hemisphere G 3.6 mm, hemisphere A 5.6 mm, hemisphere G 5.6 mm, hemisphere A 7.5 mm, hemisphere G 7.5 mm, hemisphere A 9.5 mm, hemisphere G 9.5 mm, hemisphere A 11.4 mm, and hemisphere G 11.4 mm. Figure 2 shows photographs of simple experimental models and a schematic representation. The process of recording the ultrasound images at 5 MHz and then 9 MHz in these 10 different hemispherical objects was repeated 10 times to obtain a total of 200 images.

The acquired images were sent to a personal computer, and the echo intensity of the vertical artifact was measured using a dedicated prototype software program developed with Visual Studio C++[16]. This program imports LOGIQ S8 still images with several imaging parameters, including the dynamic range, gain, and grayscale map, so that the brightness of each pixel is compensated to a normalized decibel value [dB]. The main functions of the program are as follows: (1) show a graph of the echo intensity to the depth direction, where the calculated value at each depth becomes an average depending on the size of the region of interest (ROI) (as shown in Figs. 3 and 4); (2) calculate the mean echo intensity in the ROI; and (3) estimate the

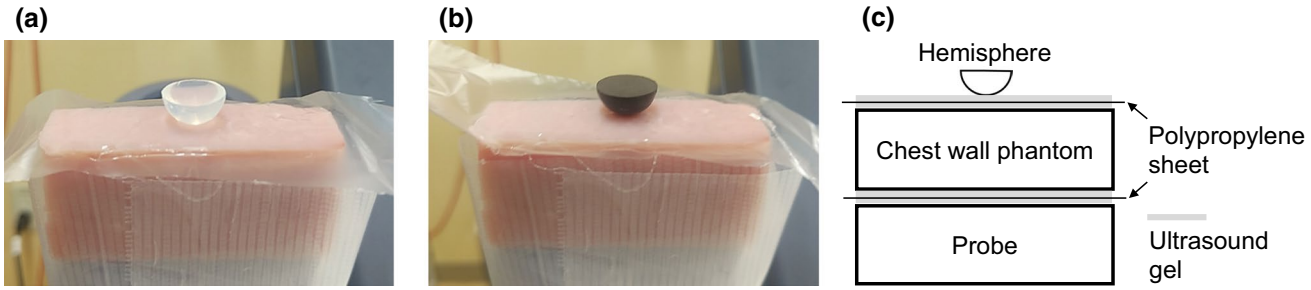

Fig. 2 Photographs of simple experimental models using hemisphere A (**a**) and hemisphere G (**b**) (diameter: 11.4 mm) and a schematic representation (**c**)

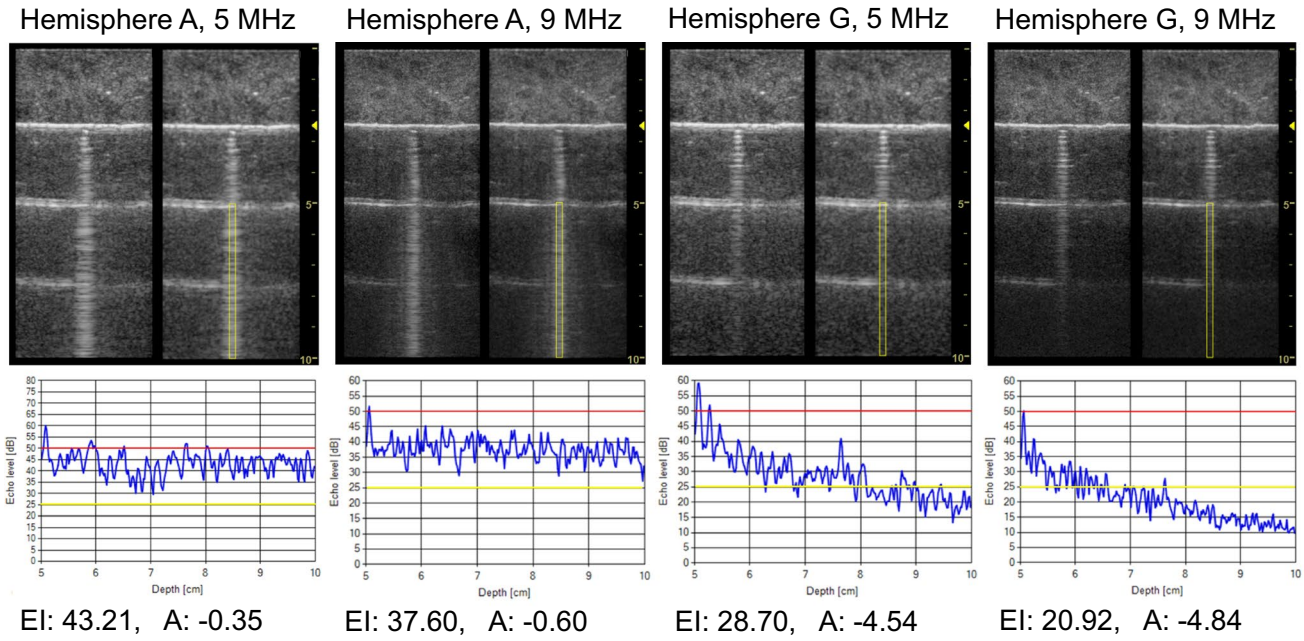

Fig. 3 Ultrasonograms obtained at 5 and 9 MHz in hemisphere A and hemisphere G 3.6 mm in diameter along with corresponding graphs illustrating the relationship between the depth (cm) and the echo intensity (dB) in the region of interest (yellow rectangle on the ultrasonogram). EI and A represent the average echo intensity and attenuation, respectively

attenuation of the sound [dB/cm] by measuring the decay slope from the graph using the least squares method. With this graph, we were able to check the saturation based on a clip of the signals. The chest wall phantom seemed to have adequate attenuation. As a result, the obtained signals were considered not to be saturated. Because an image pixel is affected by post-image processing, ultrasound images were acquired without image processing (e.g., speckle reduction imaging [SRI] filter, frame averaging, and special compound imaging).

In our previous study, we established the width of ROIs via three different methods to measure the echo intensity of vertical artifacts, and we found that no significant differences were observed between these methods when comparing the echo intensity [16]. Therefore, we selected just one of the methods for use in the present study, as follows. First, the minimal width of the bars of the vertical artifacts was determined among a total of 200 ultrasound images. Transverse lines projecting from the bar of the vertical artifact were not included in the width of the artifacts. All ROIs were then manually set at the center of the bars of the vertical artifacts at the same minimal width and at a depth of 5–10 cm. The vertical artifacts at 2.5–5 cm in depth were not included in ROIs as in the previous study since the hypoechoic images of the larger objects are shown just under 2.5 cm in depth [16]. On top of that, the visibility of vertical artifacts does not always start just under the real image of the objects in actual patients. Demi et al. hypothesized that the magnitude of the mirror effects at the pleural plane can be higher than that of the vertical artifacts, and that the latter can be

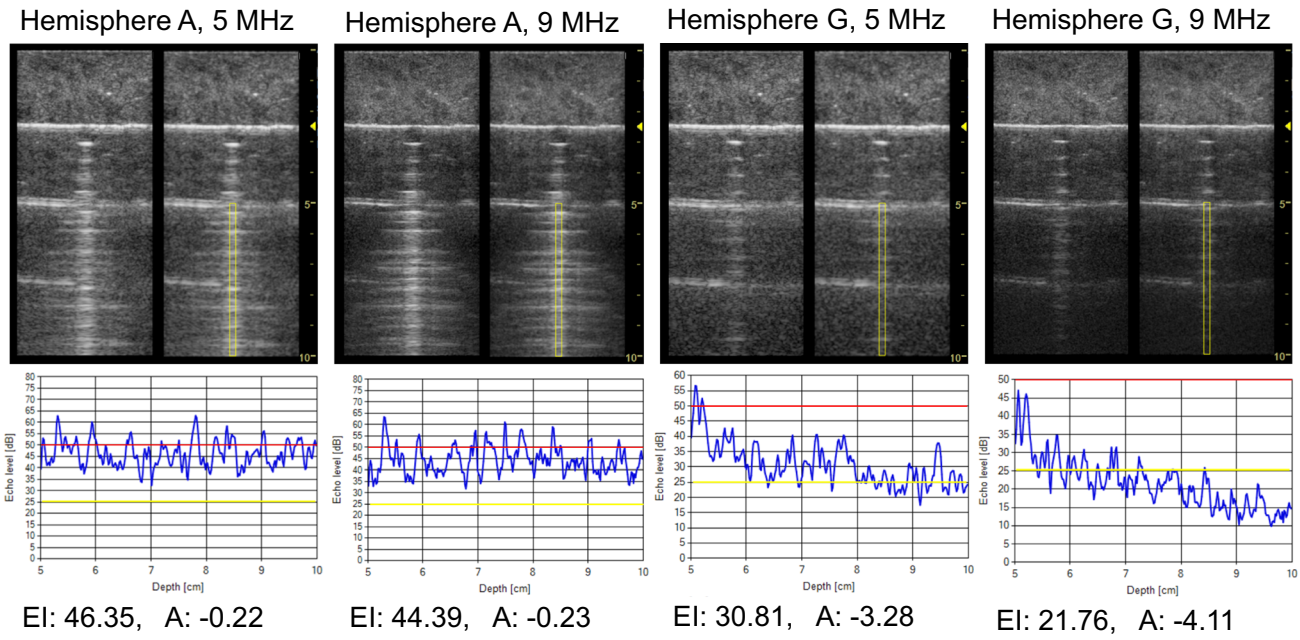

Fig. 4 Ultrasonograms obtained at 5 and 9 MHz in hemisphere A and hemisphere G 11.4 mm in diameter along with corresponding graphs illustrating the relationship between the depth (cm) and the echo intensity (dB) in the region of interest (yellow rectangle on the ultrasonogram). EI and A represent the average echo intensity and attenuation, respectively

initially masked between the pleural line and the first A-line [12]. If the deep side of the bar of the artifact was not clear or had vanished, the sides of the rectangular ROIs were set based on the superficial sides of the bar. The average echo intensity values and the attenuation values inside the ROI on the ultrasound images per object were used for the analyses.

Statistical analyses

The average echo intensity values and the attenuation values were summarized by each hemispherical object using medians, ranges, and means. Wilcoxon's rank-sum test was used to compare the echo intensity and attenuation between hemispheres A and G at each size and frequency. Differences in the echo intensity between 5 and 9 MHz were compared between hemispheres A and G at each size using the same test.

Diagnostic ultrasound scanners are built to compensate for attenuation by increasing the brightness according to the depth within the body as TGC by default. The compensation is adjusted by each manufacturer to be stronger when selecting higher frequencies. In this sense, we needed to cancel the effect of the default TGC to investigate the "true" difference (rather than the difference shown on the screen) in echo intensity or attenuation between frequencies. To investigate the differences in the echo intensity influenced by the attenuation inside hemisphere G between 5 and 9 MHz, the differences between the median echo intensity values obtained from hemisphere A and each echo intensity value obtained from hemisphere G were calculated for each size. The differences between 5 and 9 MHz in hemisphere G were then compared using Wilcoxon's rank-sum test for each size.

The Kruskal–Wallis test was used to compare the echo intensities among five sizes (3.6, 5.6, 7.5, 9.5, and 11.4 mm in diameter) in images of hemisphere A obtained at 5 MHz, hemisphere A at 9 MHz, hemisphere G at 5 MHz, and hemisphere G at 9 MHz. We next compared the echo intensities between 3.6 and 11.4 mm in diameter with Wilcoxon's rank-sum test as post-hoc analyses.

These statistical analyses were two-sided, with $P < 0.05$ considered statistically significant. The analyses were carried out using the STATA version 13.1 software program (StataCorp LP, College Station, TX, USA).

Results

Table 2 summarizes the basic results of the statistical analyses of the echo intensities (dB) obtained from the ROIs in hemispheres A and G for each frequency and diameter, along with the differences between frequencies at each diameter. Table 3 shows the results of the analyses of the difference between the median echo intensity values obtained from hemisphere A and each echo intensity value obtained from hemisphere G for each frequency and diameter. Table 4 summarizes the basic results of the analyses

Table 2 Echo intensity value (dB) obtained from the region of interest in hemisphere A and hemisphere G at each diameter

	Hemisphere A			Hemisphere G		
	5 MHz	9 MHz	Difference	5 MHz	9 MHz	Difference
3.6 mm						
Median	41.18	38.15	2.75	28.89	20.34	7.99
Range	36.81, 48.08	33.89, 47.33	0.75, 5.61	25.00, 31.74	17.10, 22.62	7.58, 11.04
Mean	41.32	38.63	2.69	28.33	19.83	8.50
5.6 mm						
Median	44.10	41.70	2.20	29.38	20.88	9.06
Range	36.59, 47.12	32.37, 47.29	-1.87, 4.93	27.77, 30.62	18.04, 22.00	6.70, 9.91
Mean	43.39	41.29	2.10	29.29	20.69	8.59
7.5 mm						
Median	44.27	41.60	2.48	30.04	21.77	8.29
Range	38.97, 54.63	36.30, 53.61	0.63, 5.83	28.47, 32.75	19.65, 26.02	6.43, 8.82
Mean	44.56	42.18	2.39	30.31	22.30	8.01
9.5 mm						
Median	43.60	42.20	1.86	29.86	21.91	7.91
Range	41.83, 49.30	37.60, 47.58	0.97, 4.23	26.39, 33.54	17.79, 25.11	6.58, 8.60
Mean	44.33	42.15	2.18	29.72	21.92	7.80
11.4 mm						
Median	46.25	44.76	2.03	31.12	22.04	8.63
Range	43.67, 50.73	41.56, 51.81	-1.08, 4.59	28.45, 34.94	19.88, 26.73	7.89, 11.06
Mean	46.60	44.77	1.82	31.52	22.63	8.89

Hemisphere A = Hemispherical gel object made of water and agar

Hemisphere G = Hemispherical gel object made of water, agar, and graphite

Table 3 The difference between the median of echo intensity values obtained from hemisphere A and each echo intensity value obtained from hemisphere G (dB)

	5 MHz	9 MHz
3.6 mm		
Median	12.30	17.82
Range	9.44, 16.18	15.53, 21.05
Mean	12.85	18.32
5.6 mm		
Median	14.73	20.83
Range	13.48, 16.33	19.70, 23.66
Mean	14.81	21.01
7.5 mm		
Median	14.23	19.83
Range	11.52, 15.80	15.58, 21.95
Mean	13.96	19.29
9.5 mm		
Median	13.24	20.30
Range	10.06, 17.21	17.09, 24.41
Mean	13.88	20.28
11.4 mm		
Median	15.13	22.73
Range	11.31, 17.80	18.03, 24.88
Mean	14.73	22.14

of the attenuation (dB/cm) obtained by linearization with a least-squares method in each graph, illustrating the relationship between the depth (cm) and the corresponding echo intensity (dB) in the ROI. Figure 3 shows examples of ultrasonograms obtained at 5 and 9 MHz in hemisphere A and hemisphere G 3.6 mm in diameter along with corresponding graphs illustrating the relationship between the depth and echo intensity in the ROI. Figure 4 shows examples of ultrasonograms in hemisphere A and hemisphere G 11.4 mm in diameter along with corresponding graphs.

At all sizes, the echo intensities at 5 and 9 MHz in hemisphere G were significantly lower than those at 5 and 9 MHz in hemisphere A of the same size (Table 2 and Electronic Supplementary Material 1–5, $p < 0.001$). The attenuations at 5 and 9 MHz in hemisphere G were significantly larger than those at 5 and 9 MHz in hemisphere A of the same size (Table 4, $p < 0.001$). The differences in echo intensities between 5 and 9 MHz in hemisphere G were significantly larger than those in hemisphere A of the same size (Table 2 and Electronic Supplementary Material 6, $p < 0.001$). The differences between the median echo intensity values obtained from hemisphere A and each echo intensity value obtained from hemisphere G at 9 MHz were significantly larger than those at 5 MHz (Table 3 and Electronic Supplementary Material 7, $p < 0.001$).

Table 4 Attenuation (dB/cm) obtained by linearization with a least-squares method of each graph illustrating the relationship between the depth (cm) and the corresponding echo intensity (dB) in the region of interest

	Hemisphere A		Hemisphere G	
	5 MHz	9 MHz	5 MHz	9 MHz
3.6 mm				
Median	−0.63	−0.71	−3.70	−3.84
Range	−1.70, 0.41	-2.13, 0.48	−4.54, -2.96	−4.84, -3.52
Mean	−0.71	−0.67	−3.73	−3.97
5.6 mm				
Median	0.08	−0.01	−3.73	−3.78
Range	−1.34, 0.55	−1.03, 0.87	−4.48, -3.36	−4.42, −3.51
Mean	−0.06	−0.01	−3.79	−3.88
7.5 mm				
Median	−0.55	0.08	−3.44	−4.11
Range	−0.86, 0.57	−0.88, 1.09	−4.38, −2.75	−4.41, −3.53
Mean	−0.11	0.02	−3.53	−3.99
9.5 mm				
Median	−0.36	−0.35	−3.69	−4.04
Range	−1.09, 0.49	−0.75, 0.62	−4.50, -2.43	−4.81, -3.12
Mean	−0.28	−0.35	−3.61	−4.05
11.4 mm				
Median	0.10	0.17	−3.39	−4.04
Range	−0.56, 2.29	−0.23, 2.29	−3.99, −2.40	−4.67, −3.33
Mean	0.38	0.50	−3.34	−4.00

There were significant differences in echo intensities between at least two of the five sizes on images of hemisphere A obtained at 5 MHz (Table 2, $p = 0.022$), hemisphere A at 9 MHz ($p = 0.028$), hemisphere G at 5 MHz ($p = 0.015$), and hemisphere G at 9 MHz ($p = 0.026$). The echo intensity for 11.4 mm was higher than that for 3.6 mm on images of hemisphere A obtained at 5 MHz ($p = 0.002$), hemisphere A at 9 MHz ($p = 0.003$), hemisphere G at 5 MHz ($p = 0.009$), and hemisphere G at 9 MHz ($p = 0.023$).

Discussion

The mechanisms underlying vertical artifacts in lung ultrasound have been gradually revealed owing to researchers' enormous efforts. To our knowledge, there have been no in vitro studies showing the relationship of the attenuation inside acoustic traps with the characteristics of vertical artifacts.

In the present experimental study using simple models, we found that the echo intensities and attenuations of the vertical artifacts were affected by the attenuation inside the traps based on our comparison of the vertical artifacts generated by hemispherical gel objects with different attenuation coefficients. At each size, the echo intensities in the vertical artifacts generated from hemisphere G (agar containing graphite) were significantly lower than those in the artifacts generated from hemisphere A (pure agar) with the same machine settings. The attenuation coefficient within hemisphere G was 0.5 dB/cm · MHz, but the attenuation was observed to be quite small within hemisphere A. In addition, the attenuations in hemisphere G were significantly larger than those in hemisphere A.

The terms "intensity" and "attenuation" in the results are different indices, but they are closely related to each other. In addition, these indices can indirectly capture the length of vertical artifacts. Our results showed that the physical composition of the acoustic traps affected the intensity and length of vertical artifacts. These results are consistent with a previous clinical study. Mento et al. [13] demonstrated that the mean total intensity of B-lines representing fibrotic patients was significantly lower than the mean value in nonfibrotic patients, a difference they suspected was likely associated with the physical composition of acoustic traps.

Recent experimental and clinical studies have demonstrated the influence of frequency on the generation, configuration, and intensity of vertical artifacts [8, 9, 13, 20–23]. In the present study, we focused on the influence of frequencies on the intensities of vertical artifacts generated from objects with an attenuation coefficient similar to soft tissue (0.5 dB/cm · MHz). For each size, the differences in echo intensities between 5 and 9 MHz in hemisphere G were significantly larger than those in hemisphere A, indicating that the intensity of the vertical artifact generated from the acoustic trap with an attenuation coefficient similar to that of soft tissue decreased significantly on the screen of the diagnostic ultrasound scanner when the frequency was changed from 5 to 9 MHz. These results are consistent with a previous clinical study. Using another diagnostic ultrasound scanner, Buda et al. [8] demonstrated that changing the frequency from 2 to 6 MHz led to the shortening or disappearance of vertical artifacts, and this phenomenon was more characteristic of pulmonary fibrosis than cardiogenic pulmonary edema. These results provide clinicians with useful information when interpreting the echo intensity and length of vertical artifacts in clinical settings.

However, the results obtained from diagnostic scanners must be cautiously interpreted from an acoustics perspective. As mentioned above, diagnostic ultrasound scanners are built to compensate for attenuation by increasing the brightness according to the depth as the TGC by default. This compensation is adjusted to be stronger when selecting higher frequencies by each manufacturer. We also investigated the differences in echo intensity influenced by the attenuation inside hemisphere G between 5 and 9 MHz by cancelling the effect of the default TGC using a calculation. The differences between the median echo intensity values

obtained from hemisphere A and each echo intensity value obtained from hemisphere G at 9 MHz were significantly larger than those at 5 MHz, indicating that the echo intensity of the vertical artifacts generated from the acoustic trap with the attenuation coefficient truly decreased significantly when the frequency was changed from 5 to 9 MHz. This finding supports the notion that analyzing vertical artifacts by employing two different (extreme) frequencies may help better estimate the physical composition of the acoustic traps and be useful for differentiating pulmonary edema from interstitial lung diseases [8]. Assessment of the characteristics of vertical artifacts seems to be promising; however, an objective measurement of echo intensity or length of vertical artifacts should be developed and deployed in diagnostic ultrasound scanners.

In our previous study, objects of different shapes made using gel balls 1 cm in diameter were used as acoustic traps to measure and compare the echo intensities of vertical artifacts. For a given shape, the intensity was markedly higher in the model with a point of contact than in the model with a plane of contact. With the same point or plane of contact, the echo intensity was higher in the taller or larger model than in the smaller one [16]. Therefore, in an acoustic trap with a small aperture, the ultrasound energy would have greater difficulty escaping, and opportunities for reflection within the trap would consequently increase. In the case of a larger trap volume, with an aperture measuring the same size, the ultrasound energy would still have difficulty escaping, and opportunities for reflection would consequently increase. In the present study, we used hemispherical gel objects with five different diameters. As the size or diameter increased, the curvature decreased, and the actual point of contact (size of the channel) consequently increased. In this regard, the difference in echo intensities between hemispherical gel objects of different sizes could not be interpreted as simply as in our previous study in which gel objects of different sizes with the same curvature had been used for comparison [16]. The difference was not necessarily observed between objects of different sizes. Notably, the echo intensity in the 11.4-mm sample (the largest one) was higher than that in the 3.6-mm sample (the smallest one) on images of hemisphere A obtained at 5 MHz, hemisphere A at 9 MHz, hemisphere G at 5 MHz, and hemisphere G at 9 MHz. This experiment also shows that the size of the acoustic trap is a factor influencing the echo intensity of vertical artifacts. On top of that, the echo intensity seems to be determined by the ratio of the size of the acoustic trap to the size of the point of contact. The intensities of vertical artifacts generated from objects with a significant attenuation coefficient and different sizes with the same point of contact also need to be compared in future studies.

Our series of studies and other previous studies have shown that the intensity, attenuation, and length of vertical artifacts depend on many factors, such as the relative size of the acoustic channels to trap volume, the physical components of the traps, and the ultrasound machine settings [23]. Thus, a simple characterization of vertical artifacts can be misleading [19]. In future clinical studies related to these topics, a certain degree of standardization of machine settings for lung ultrasound should be implemented [11, 18, 19, 23].

Several limitations associated with the present study warrant mention. Simple experimental models were used to represent pathologic changes in the subpleural area. However, actual acoustic traps may have complicated shapes and consist of multiple components. When selecting the sizes of hemispherical gel objects, we crafted hemispherical gel objects that were 3.6, 5.6, 7.5, 9.5, and 11.4 mm in diameter and had nearly equal intervals using commercially available molds. Smaller objects similar to the sources of vertical artifacts in the lung may be more ideal, but the objects we selected were presumed to be suitable substitutes for sources based on our previous studies [9, 16]. Using a three-dimensional (3D) printer, objects with various sizes and shapes can be made, which may be useful for future analyses of vertical artifacts [19]. Regarding the selection of an ultrasound scanner, we used a commercially available diagnostic scanner for this experimental study. When using this scanner, we needed to apply correction to cancel the effect of TGC by default. Having access to a programmable ultrasound scanner for basic research purposes might have been better, allowing us to control more presets, such as the default TGC, and elucidate the physical basis of vertical artifacts [23]. However, basic research using diagnostic scanners is also useful for clarifying the mechanisms underlying phenomena observed using scanners in clinical settings. Regarding the selection of frequencies, we only used the frequencies of 5 and 9 MHz with a linear transducer. Lower-frequency transducers are often used to evaluate vertical artifacts, including B-lines and short vertical artifacts (comet tail artifacts) [8, 11]; therefore, another experimental study involving lower-frequency transducers should be considered. Regarding the measurement of the intensity and attenuation of vertical artifacts, the parts of reverberation artifacts that occurred between the footprint of the probe and the bottom of the chest wall phantom had to be included in the ROIs. The software program could not eliminate the element of the reverberation artifacts when measuring the intensity and attenuation of the vertical artifacts. However, the aim of this study was the relative assessment of the intensity and attenuation; thus, the limitation did not directly affect the conclusions.

Conclusions

Using simple experimental models for lung ultrasound, we evaluated the relationship of the attenuation inside the sources of vertical artifacts with the echo intensity and

attenuation of the artifacts. As sources of the artifacts, we crafted hemispherical gel objects using two different mediums (pure agar or agar containing graphite) and five different diameters. The attenuation coefficient of agar-containing graphite was similar to that of soft tissue. The echo intensity and attenuation of the vertical artifact generated from each object were measured and compared. For all sizes, the intensity and attenuation of the artifacts in the objects made of agar containing graphite were significantly lower and larger, respectively, than those in the objects with pure agar. In the objects containing graphite, the intensity significantly decreased when the frequency was changed from 5 to 9 MHz. Based on the present findings, assessing the intensity and attenuation of vertical artifacts may be useful for estimating the physical composition of sources of vertical artifacts and for differentiating pathologies in lung ultrasound. Further experimental and clinical studies are still needed to elucidate the mechanism in vertical artifacts, including B-lines and comet tail artifacts.

Supplementary Information The online version contains supplementary material available at https://doi.org/10.1007/s10396-022-01244-0.

Acknowledgements This study received no financial support for the conduct of the experiments or preparation of the article.

Declarations

Conflict of Interest All authors declare no competing interests.

Ethical statements This article does not contain any studies with human or animal subjects performed by any of the authors.

References

1. Volpicelli G, Elbarbary M, Blaivas M, et al. International evidence-based recommendations for point-of-care lung ultrasound. Intensive Care Med. 2012;38:577–91.
2. Pellicori P, Platz E, Dauw J, et al. Ultrasound imaging of congestion in heart failure: examinations beyond the heart. Eur J Heart Fail. 2021;23:703–12.
3. Chiumello D, Umbrello M, Sferrazza Papa GF, et al. Global and regional diagnostic accuracy of lung ultrasound compared to CT in patients with acute respiratory distress syndrome. Crit Care Med. 2019;47:1599–606.
4. Gargani L, Romei C, Bruni C, et al. Lung ultrasound B-lines in systemic sclerosis: cut-off values and methodological indications for interstitial lung disease screening. Rheumatology (Oxford). 2021. https://doi.org/10.1093/rheumatology/keab801.
5. Wang Y, Gargani L, Barskova T, et al. Usefulness of lung ultrasound B-lines in connective tissue disease-associated interstitial lung disease: a literature review. Arthritis Res Ther. 2017;19:206.
6. Kameda T, Mizuma Y, Taniguchi H, et al. Point-of-care lung ultrasound for the assessment of pneumonia: a narrative review in the COVID-19 era. J Med Ultrason. 2021;48:31–43.
7. Volpicelli G, Gargani L, Perlini S, et al. Lung ultrasound for the early diagnosis of COVID-19 pneumonia: an international multicenter study. Intensive Care Med. 2021;47:444–54.
8. Buda N, Skoczylas A, Demi M, et al. Clinical impact of vertical artifacts changing with frequency in lung ultrasound. Diagnostics. 2021;11:401.
9. Kameda T, Kamiyama N, Kobayashi H, et al. Ultrasonic B-line-like artifacts generated with simple experimental models provide clues to solve key issues in B-Lines. Ultrasound Med Biol. 2019;45:1617–26.
10. Volpicelli G, Gargani L. Interstitial syndrome. In: Mathis G, editor. Chest sonography. 4th ed. Cham (Switzerland): Springer; 2017. p. 45–50.
11. Mathis G, Horn R, Morf S, et al. WFUMB position paper on reverberation artifacts in lung ultrasound: B-lines or comet-tails? Med Ultrason. 2021;23:70–3.
12. Demi M, Prediletto R, Soldati G, et al. Physical mechanisms providing clinical information from ultrasound lung images: hypotheses and early confirmations. IEEE Trans Ultrason Ferroelectr Freq Control. 2020;67:612–23.
13. Mento F, Soldati G, Prediletto R, et al. Quantitative lung ultrasound spectroscopy applied to the diagnosis of pulmonary fibrosis: The first clinical study. IEEE Trans Ultrason Ferroelectr Freq Control. 2020;67:2265–73.
14. Lichtenstein D, Mézière G, Biderman P, et al. The comet-tail artefact. An ultrasound sign of alveolar-interstitial syndrome. Am J Respir Crit Care Med. 1997;156:1640–6.
15. Soldati G, Demi M, Inchingolo R, et al. On the physical basis of pulmonary sonographic interstitial syndrome. J Ultrasound Med. 2016;35:2075–86.
16. Kameda T, Kamiyama N, Taniguchi N. Simple experimental models for elucidating the mechanism underlying vertical artifacts in lung ultrasound: tools for revisiting B-lines. Ultrasound Med Biol. 2021;47:3543–55.
17. Demi M. On the replica of US pulmonary artifacts by means of physical models. Diagnostics (Basel). 2021;11:1666.
18. Kameda T, Kamiyama N, Taniguchi N. The mechanisms underlying vertical artifacts in lung ultrasound and their proper utilization for the evaluation of cardiogenic pulmonary edema. Diagnostics (Basel). 2022;12:252.
19. Demi M. The impact of multiple concurrent factors on the length of the ultrasound pulmonary vertical artifacts as illustrated through the experimental and numerical analysis of simple models. J Acoust Soc Am. 2021;150:2106.
20. Demi L, van Hoeve W, van Sloun RJG, et al. Determination of a potential quantitative measure of the state of the lung using lung ultrasound spectroscopy. Sci Rep. 2017;7:12746.
21. Demi L, Demi M, Prediletto R, et al. Real-time multi-frequency ultrasound imaging for quantitative lung ultrasound - first clinical results. J Acoust Soc Am. 2020;148:998.
22. Mento F, Demi L. On the influence of imaging parameters on lung ultrasound B-line artifacts, in vitro study. J Acoust Soc Am. 2020;148:975.
23. Mento F, Demi L. Dependence of lung ultrasound vertical artifacts on frequency, bandwidth, focus and angle of incidence: An in vitro study. J Acoust Soc Am. 2021;150:4075.